Synthesis and CO_2 Photoreduction of Lead-Free Cesium Bismuth Halide Perovskite Nanocrystals

Daofu Wu[a], Xusheng Zhao[a], Yanyi Huang[a], Junan Lai[a], Jiayu Yang[b], Changqing Tian[b], Peng He[a,], Qiang Huang[b,]*, Xiaosheng Tang[a,b,c,]**

[a] Key Laboratory of Optoelectronic Technology & Systems, Ministry of Education, Chongqing University, Chongqing 400044, China

[b] College of Optoelectronic Engineering, Chongqing University of Posts and Telecommunications, Chongqing 400065, China

[c] School of Materials Science and Engineering, Zhengzhou University, Zhengzhou 450001, China

*** Corresponding author.**

E-mail: xstang@cqu.edu.cn (X. Tang), qhuang1986@163.com (Q. Huang), penghe@cqu.edu.cn(P. He).

EXPERIMENTAL SECTION

Materials. $BiBr_3$ (99%, Alfa Aesar), BiI_3 (98%, Aladdin), $BiCl_3$ (analytical pure, Aladdin), CsI (99.9%, Aladdin), CsBr (99.9%, Aladdin), CsCl (99%, Aladdin), oleic acid (90%, Sigma-Aldrich), n-Octylamine (99%, Aladdin), oleylamine (90%, Energy Chemical), tri-n-octylphosphine (90%, Alfa Aesar), 1,2-ethanedithiol (98+%, Alfa Aesar), tolune (analytical pure, Sinopharm Chemical Reagent Co., Ltd, China), acetone (analytical pure, Sinopharm Chemical Reagent Co., Ltd, China), isopropanol (High performance liquid chromatography pure, Kermel, China), dimethyl sulfoxide (>99%, Sinopharm Chemical Reagent Co., Ltd, China), N,N-Dimethylformamide (High performance liquid chromatography pure, Kermel, China). All materials were used as received without further purification.

Synthesis of $Cs_3Bi_2X_9$ NCs. For $Cs_3Bi_2Cl_9$ NCs, the dissolution of 15.2 mg CsCl and 18.9 mg $BiCl_3$ with molar proportion 3:2 was made in DMSO to produce the precursor solution, and then the addition of 200 μL precursor solution into acetone was made dropwise while vigorous stirring. To synthesize ligand free $Cs_3Bi_2Br_9$ NCs, the dissolution of 19.2 mg CsBr and 26.9 mg $BiBr_3$ was made in 2 mL DMSO to form $Cs_3Bi_2Br_9$ precursor solution. The injection of 200 μL precursor solution into 5 mL isopropanol was made while vigorous stirring. For $Cs_3Bi_2I_9$, the dissolution of 23.4 mg CsI and 35.4 mg BiI_3 with molar ratio 3:2 was made in DMF for the generation of the precursor solution, and then the addition of 200 μL precursor solution into toluene was made dropwise while vigorous stirring. Typically, $Cs_3Bi_2(I_{0.5}Br_{0.5})_9$ and $Cs_3Bi_2(Cl_{0.5}Br_{0.5})_9$) were dissolved in DMSO to form precursor solution. The anti-solvent for $Cs_3Bi_2(I_{0.5}Br_{0.5})_9$ and $Cs_3Bi_2(Cl_{0.5}Br_{0.5})_9$) was isopropanol.

Characterization. X-ray diffraction (XRD) spectra of the samples was decided by powder X-ray diffraction (XRD) with Cu Ka radiation (MADZU, Japan). The transmission electron microscopy (TEM) and high-resolution transmission electron microscopy (HRTEM) were examined on ZEISS LIBRA 200FE. The UV-visible absorption spectrum was determined by the scan UV-vis spectrophotometer (UV-2100)

(Shima dzu, Japan) with a range of 300 to 800 nm. X-ray photoelectron spectroscopy (XPS) determined the chemical states of samples on ESRCALAB250Xi, Thermo Fisher Scientific. The binding energies were referenced to the C 1s peak at a binding energy of 284.8 eV. The photoluminescence (PL) spectrum was recorded on a photoluminescence spectrometer (Cary Eclipse G9800A, Agilent Technologies) from 400 to 600 nm, under an excitation wavelength of 365 nm. In an isotope labelling experiment, the CO products were detected by differentially pumped quadrupole mass spectrometer (QMS, Hiden HPR20).

Photocatalytic CO_2 Reduction. Photocatalytic CO_2 decrease was carried out at the Labsolar-6A system (Perfect Light Co., China). Meanwhile, the system is made up of a fully-enclosed quartzose reactor, a 300 W Xe lamp, and gas chromatography (GC). Before carrying out catalysis, the Xe lamp was configured with 420 nm filter for the simulation of the visible solar light illumination. The measurements were carried out within a 40 mL sealed Pyrex bottle filled with CO_2 and H_2O vapor. During the representative progress, the ultrasonic dispersion of 3 mg photocatalyst was made in 1.0 mL toluene. Then, the mixture solution was applied onto a glass (2.0 * 2.0 cm) and heated to 100 ℃ in ambient atmosphere for 0.5 hours to remove the extraneous toluene. The treated clean sample films and 10 μL water were put into the bottle which was degassed repeatedly to remove air and then filled with CO_2. In the reaction, the analysis of gaseous products collected was made per hour by a gas chromatography.

Photoelectrochemical characterizations. The NCs thin film was fabricated by spin-coated process. The ITO substrates were cleaned by sonicating sequentially in deionized water, alcohol and acetone, each for 10 min. The NCs toluene suspension was then spin-coated on the ITO substrates at 2000 rpm for 30 s. The as-prepared thin

films were subsequently dried at 60 °C on a hotplate to completely evaporate any residual supernatant. The photocurrent was performed on the CHI760e in a 3-electrode configuration with the assembled photoelectrodes (THE NCs on ITO glass) as the working electrode, the Pt mesh as the counter electrode and the Ag/AgCl electrode as the reference electrode. Filling the ethyl acetate with 0.1 M tetrabutylammonium hexafluorophosphate ($TBAPF_6$) in the cell can be taken as electrolyte. The variation of photoinduced current density versus time (i-t curve) was recorded at a 0 V bias potential under simulating sunlight switching on and off mode.

The calculation of the energy band structure. The band gap of the $Cs_3Bi_2X_9$ NCs were analyzed via the $(\alpha h\nu)^{1/2}$ versus hν curves as shown in Figure S3. The band gap (E_g) values of the $Cs_3Bi_2X_9$ (X = Cl, $Cl_{0.5}Br_{0.5}$, Br, $Br_{0.5}I_{0.5}$, I) NCs ranged from 2.01 to 3.08 eV based on the Tauc plots. The valence band (VB) edges of the $Cs_3Bi_2X_9$ (X = Cl, $Cl_{0.5}Br_{0.5}$, Br, $Br_{0.5}I_{0.5}$, I) NCs were determined by Valence-band XPS (VB XPS). As shown in Figure 2(a-e), the VB of $Cs_3Bi_2Cl_6$, $Cs_3Bi_2(Cl_{0.5}Br_{0.5})_9$, $Cs_3Bi_2Br_9$, $Cs_3Bi_{2(}Br_{0.5}I_{0.5})_9$, $Cs_3Bi_2I_9$ NCs are located at 2.67 eV, 2.15 eV, 2.13 eV, 1.36 and 1.15 respectively. Also, when we taking the bandgap values into consideration, the corresponding conduction band (CB) positions could be elucidated by the following equation: $E_{CB} = E_{VB} - E_g$. The band structures are calculated in Figure 2f, $Cs_3Bi_2(Cl_{0.5}Br_{0.5})_9$, $Cs_3Bi_2(Br_{0.5}I_{0.5})_9$ and $Cs_3Bi_2I_9$ have suitable bandgaps and energy band positions to achieve the photocatalytic CO_2-to-CO conversion.

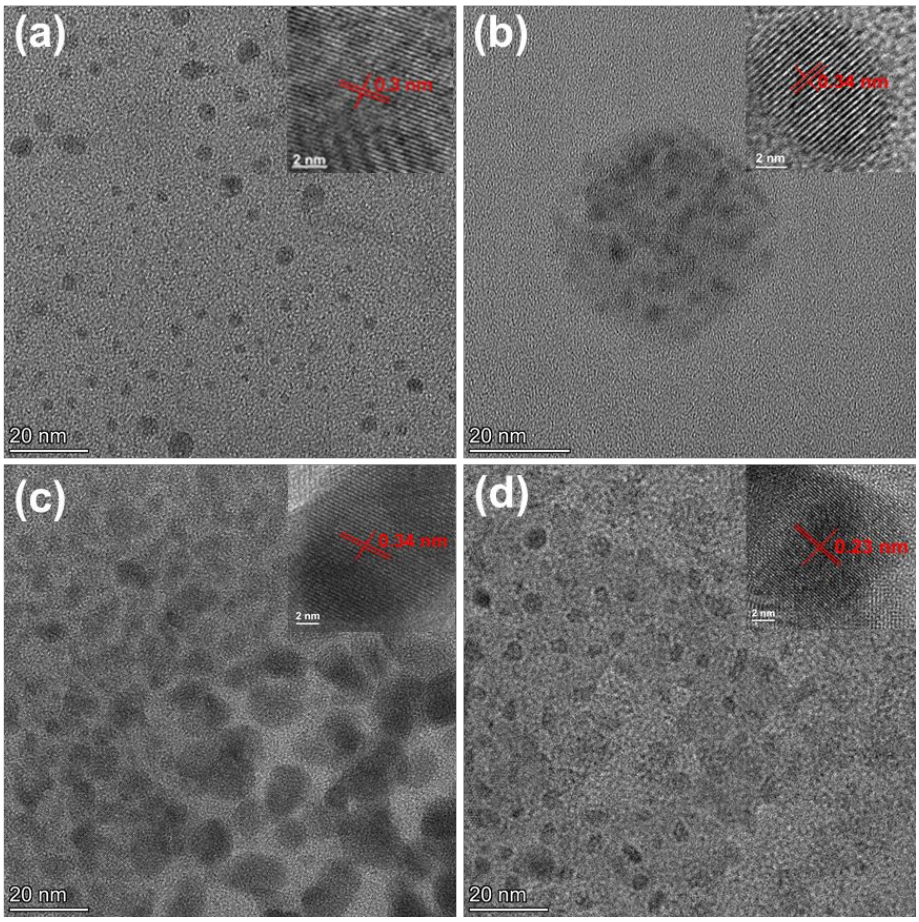

Figure S1. (a) TEM and HRTEM image of $Cs_3Bi_2Cl_9$ NCs. **(**b) TEM and HRTEM image of $Cs_3Bi_2(Cl_{0.5}Br_{0.5})_9$ NCs. (c) TEM and HRTEM image of $Cs_3Bi_2Br_9$ NCs. (d) TEM and HRTEM image of $Cs_3Bi_2I_9$ NCs.

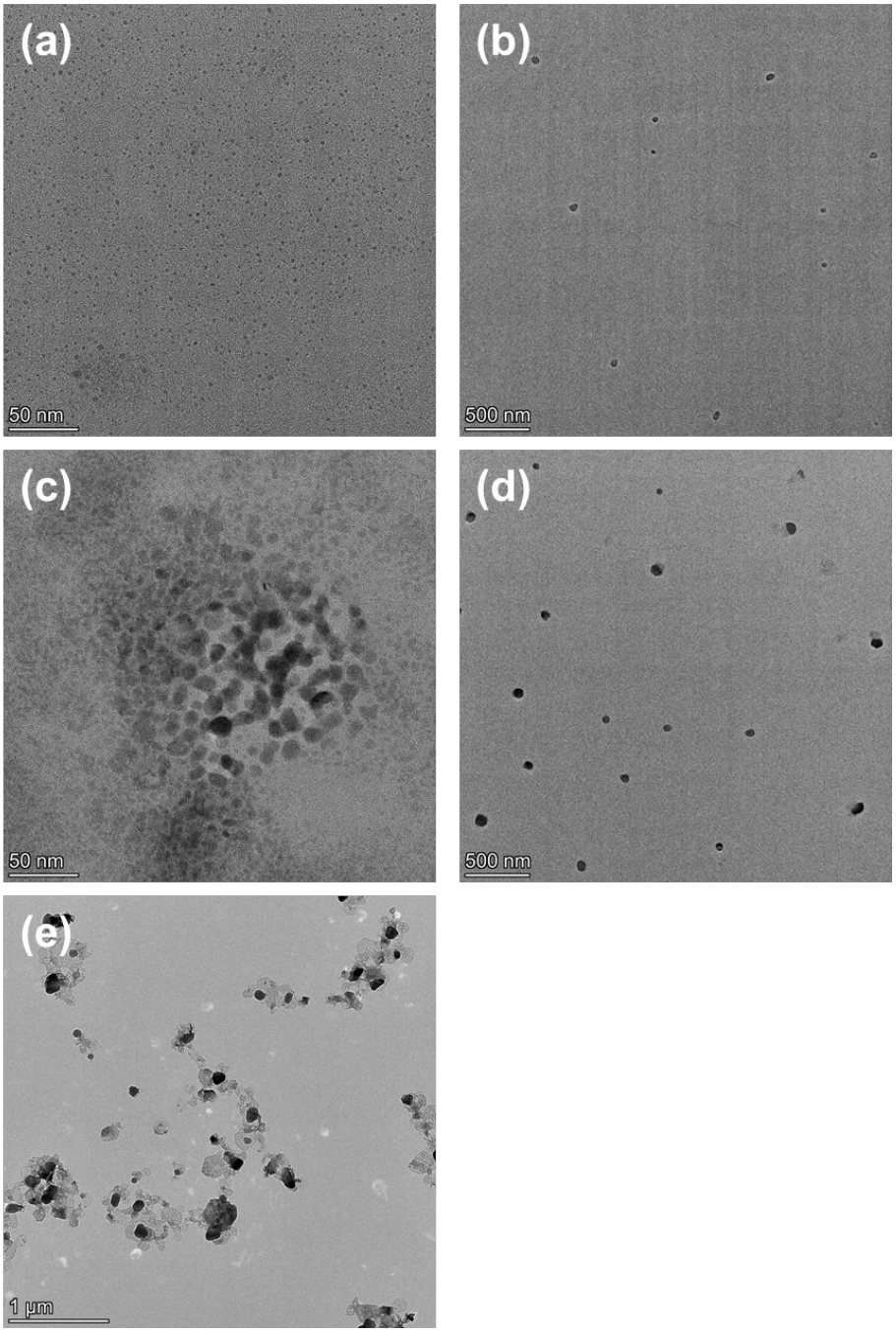

Figure S2. (a) Low-resolution TEM image of $Cs_3Bi_2X_9$ (X=Cl, $Cl_{0.5}Br_{0.5}$, Br, $Br_{0.5}I_{0.5}$, I) NCs.

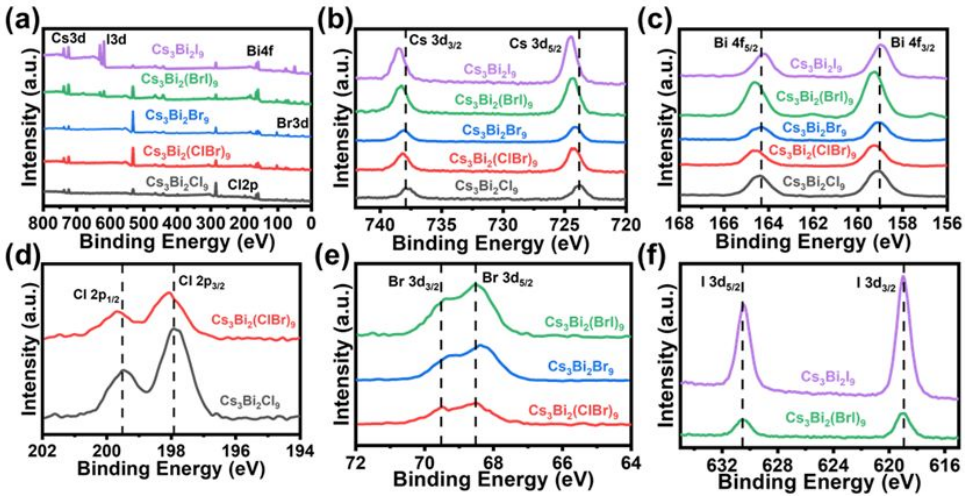

Figure S3. (a) X-ray photoelectron spectra (XPS), (b) Cs 3d, (c) Bi 4f, (d) Cl 2p, (e) Br 3d, (f) I 3d of $Cs_3Bi_2X_9$ (X=Cl, $Cl_{0.5}Br_{0.5}$, Br, $Br_{0.5}I_{0.5}$, I) NCs.

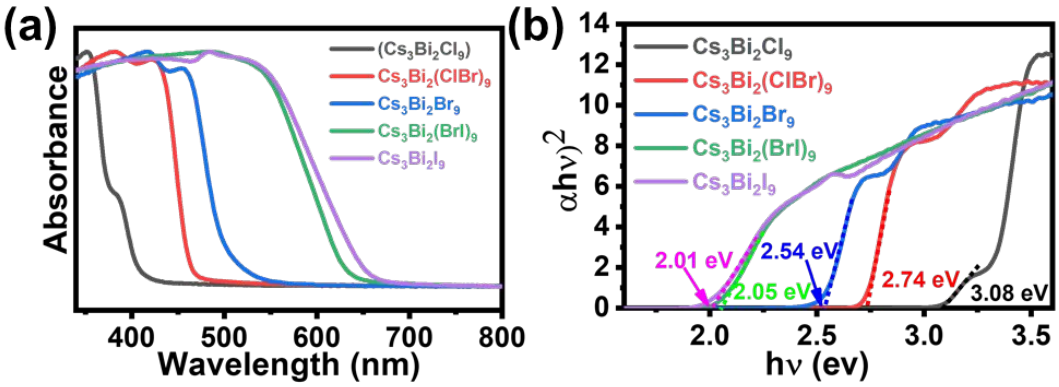

Figure S4. (a) UV–vis absorption spectra and (b) $(\alpha h\nu)^2$ versus hν curves of the $Cs_3Bi_2X_9$ (X=Cl, $Cl_{0.5}Br_{0.5}$, Br, $Br_{0.5}I_{0.5}$, I) NCs.

Table S1. Comparison of the photocatalytic CO_2 reduction activity and CO selectivity of various perovskites-based photocatalysts

Catalysts	CO/μmol $g^{-1}h^{-1}$	Selectivity/%	Cocatalyst	Model	Light	References
$Cs_3Bi_2(Br_{0.5}I_{0.5})_9$	18	100	/	gas-solid	Xe, ≥ 420 nm	This work
$Cs_3Bi_2(Cl_{0.5}Br_{0.5})_9$	16	100	/	gas-solid	Xe, ≥ 420 nm	This work
$Cs_3Bi_2I_9$	7.76	83.9	/	gas-solid	UV, 305 nm	1
$MAPbI_3$@Fe MOF	14.16	69.4	Fe MOF	ethyl acetate / water	Xe, 400 nm	2
$Cs_2AgBiBr_6$	2.35	59.9	/	ethyl acetate	AM 1.5G	3
$CsPbBr_3$/Pd	1.3	36.7	Pd	gas-solid	Xe lamp	4

Nanosheet						
$CsPbBr_3$@TiO_2	3.9	32.3	TiO_2	ethyl acetate / isopropano	AM 1.5G	5
$CsPbBr_3/C_3N_4$	148.9	71.4	C_3N_4	acetonitrile / water	Xe, ≥ 420 nm	6
$CsPbBr_3$@ZIF-67	0.5	12.8	ZIF-67	gas-solid	AM 1.5G	7
$CsPbBr_3$@GO	4.89	66.4	GO	ethyl acetate	AM 1.5G	8
$CsPbBr_3$ QDs	4.25	73.9	/	ethyl acetate / water	AM 1.5G	9
$CsPbBr_3$-Ni(tpy)	373	86.9	Ni(tpy) organic photosensitizer	ethyl acetate / water	Xe,nm ≥ 40	10
Pb-rich Ni doped $CsPbCl_3$	169.37	99	Pb, Ni	gas-solid	AM 1.5G	11
$CsPbBr_3$	32.675	68.97	/	ethyl acetate / water	Xe, 450 nm	12
$Cs_3Sn_2Br_9$	127.5	/	/	octadecene / water	AM 1.5G	13
Mn doped $CsPb(BrCl)_3$	213	95.89	Mn	ethyl acetate / water	AM 1.5G	14
Co doped $CsPbBr_3/Cs_4PbBr_6$	122.33	/	Co	acetonitrile/water/methanol	Xe, 300 W	15
$CsPbBr_3$@UiO-66(NH_2)	8.2	96.97	UiO-66(NH_2)	ethyl acetate / wate	Xe,nm ≥ 42	16
Fe doped $CsPbBr_3$	3.2	34.4	Fe	gas-solid	Xe, 400 W	17
$CsPbBr_3$/MXene	26.61	79.73	MXene	ethyl acetate / water	Xe, ≥ 420 nm	18
Co doped $CsPbBr_3$ Cs4$PbBr_6$	11.95	/	Co	pure water	Xe,nm ≥ 40	19
$CsPbBr_3/TiO_2$	12.9	/	TiO_2	ethyl acetate / water	Xe, ≥ 400 nm	20
$CsPb(Br_{0.5}Cl_{0.5})_3$	85.22	87.66	/	ethyl acetate / water	AM 1.5G	21
$Cs_3Bi_2Br_9$	26.95	98.7	/	gas-solid	AM 1.5G	22
$Cs_3Bi_2Cl_9$	21.01	98.3	/	gas-solid	AM 1.5G	22

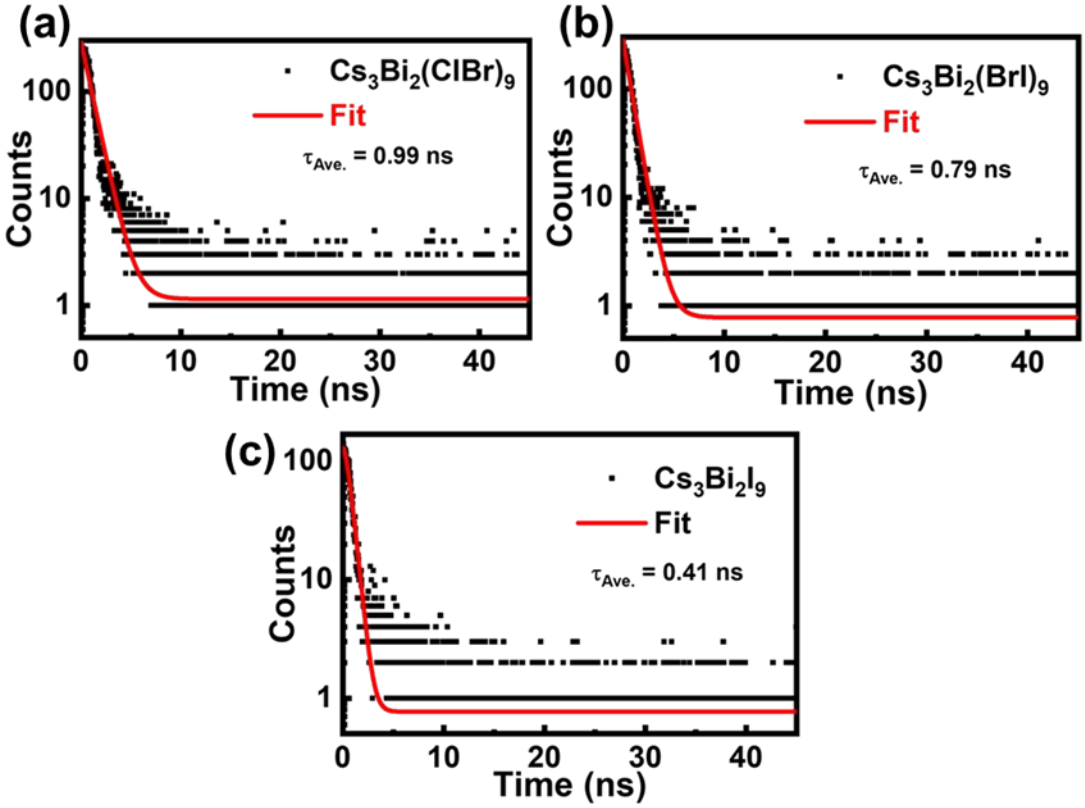

Figure S5. Time-resolved fluorescence emission decay spectra of (a) $Cs_3Bi_2(Cl_{0.5}Br_{0.5})_9$ (b) $Cs_3Bi_2(Br_{0.5}I_{0.5})_9$ and (c) $Cs_3Bi_2I_9$ NCs.

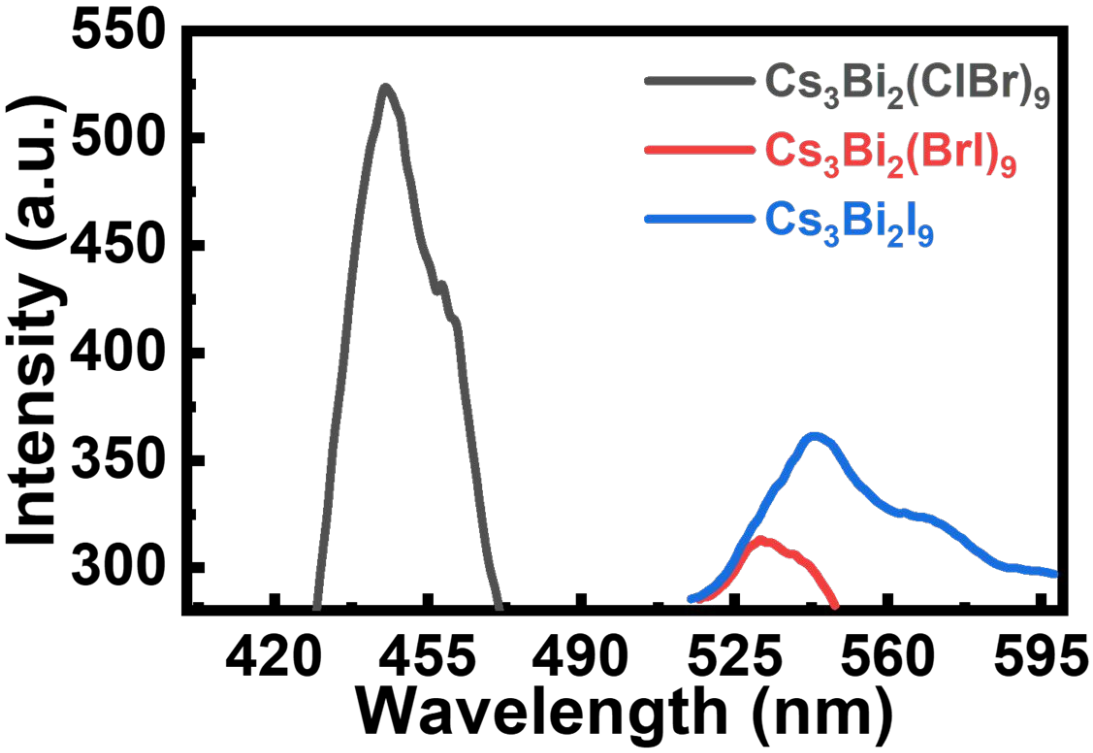

Figure S6. Photoluminescence (PL) spectra of $Cs_3Bi_2(Cl_{0.5}Br_{0.5})_9$,$Cs_3Bi_2(Br_{0.5}I_{0.5})_9$ and $Cs_3Bi_2I_9$ NCs.

Table S2. TRPL decay parameters of the $Cs_3Bi_2X_9$ (X = $Cl_{0.5}Br_{0.5}$, $Br_{0.5}I_{0.5}$, I)

	τ_1(ns)	A_1	τ_2(ns)	A_2	τ_{ave}(ns)
$Cs_3Bi_2(ClBr)_9$	0.99	151.2	0.99	101.7	0.99
$Cs_3Bi_2(BrI)_9$	0.79	387.3	0.79	48.1	0.79
$Cs_3Bi_2I_9$	0.42	144.5	0.41	-133.3	0.41

References

(1) Bhosale, S. S.; Kharade, A. K.; Jokar, E.; Fathi, A.; Chang, S. M.; Diau, E. W., Mechanism of Photocatalytic CO_2 Reduction by Bismuth-Based Perovskite Nanocrystals at the Gas-Solid Interface. *J. Am. Chem. Soc.* **2019,** *141*, 20434-20442.

(2) Wu, L. Y.; Mu, Y. F.; Guo, X. X.; Zhang, W.; Zhang, Z. M.; Zhang, M.; Lu, T. B., Encapsulating Perovskite Quantum Dots in Iron-Based Metal-Organic Frameworks (MOFs) for Efficient Photocatalytic CO_2 Reduction. *Angew. Chem. Int. Ed. Engl.* **2019,** *58*, 9491-9495.

(3) Zhou, L.; Xu, Y. F.; Chen, B. X.; Kuang, D. B.; Su, C. Y., Synthesis and Photocatalytic Application of Stable Lead-Free $Cs_2AgBiBr_6$ Perovskite Nanocrystals. *Small* **2018,** *14*, 1703762.

(4) Xu, Y.; Yang, M.; Chen, H.; Liao, J.; Wang, X.; Kuang, D., Enhanced Solar-Driven Gaseous CO_2 Conversion by $CsPbBr_3$ Nanocrystal/Pd Nanosheet Schottky-Junction Photocatalyst. *ACS Appl. Energy Mater.* **2018,** *1*, 5083-5089.

(5) Xu, Y.; Wang, X.; Liao, J.; Chen, B.; Chen, H.; Kuang, D., Amorphous-TiO_2-Encapsulated $CsPbBr_3$ Nanocrystal Composite Photocatalyst with Enhanced Charge Separation and CO_2 Fixation. *Adv. Mater. Interfaces* **2018,** *5*, 1801015.

(6) Ou, M.; Tu, W.; Yin, S.; Xing, W.; Wu, S.; Wang, H.; Wan, S.; Zhong, Q.; Xu, R., Amino-Assisted Anchoring of $CsPbBr_3$ Perovskite Quantum Dots on Porous g-C_3N_4 for Enhanced Photocatalytic CO_2 Reduction. *Angew. Chem. Int. Ed. Engl.* **2018,** *57*, 13570-13574.

(7) Kong, Z.; Liao, J.; Dong, Y.; Xu, Y.; Chen, H.; Kuang, D.; Su, C., Core@Shell $CsPbBr_3$@Zeolitic Imidazolate Framework Nanocomposite for Efficient Photocatalytic CO_2 Reduction. *ACS Energy Lett.* **2018,** *3*, 2656-2662.

(8) Xu, Y. F.; Yang, M. Z.; Chen, B. X.; Wang, X. D.; Chen, H. Y.; Kuang, D. B.; Su, C. Y., A $CsPbBr_3$ Perovskite Quantum Dot/Graphene Oxide Composite for Photocatalytic CO_2 Reduction. *J. Am. Chem. Soc.* **2017,** *139*, 5660-5663.

(9) Hou, J.; Cao, S.; Wu, Y.; Gao, Z.; Liang, F.; Sun, Y.; Lin, Z.; Sun, L., Inorganic Colloidal Perovskite Quantum Dots for Robust Solar CO_2 Reduction. *Chem. - Eur. J.* **2017,** *23*, 9481-9485.

(10) Chen, Z.; Hu, Y.; Wang, J.; Shen, Q.; Zhang, Y.; Ding, C.; Bai, Y.; Jiang, G.; Li, Z.; Gaponik, N., Boosting Photocatalytic CO_2 Reduction on $CsPbBr_3$ Perovskite

Nanocrystals by Immobilizing Metal Complexes. *Chem. Mater.* **2020,** *32*, 1517-1525.

(11) Zhu, J.; Zhu, Y.; Huang, J.; Hou, L.; Shen, J.; Li, C., Synthesis of Monodisperse Water-Stable Surface Pb-Rich $CsPbCl_3$ Nanocrystals for Efficient Photocatalytic CO_2 Reduction. *Nanoscale* **2020,** *12*, 11842-11846.

(12) Shyamal, S.; Dutta, S. K.; Das, T.; Sen, S.; Chakraborty, S.; Pradhan, N., Facets and Defects in Perovskite Nanocrystals for Photocatalytic CO_2 Reduction. *J. Phys. Chem. Lett.* **2020,** *11*, 3608-3614.

(13) Lu, C.; Itanze, D. S.; Aragon, A. G.; Ma, X.; Li, H.; Ucer, K. B.; Hewitt, C.; Carroll, D. L.; Williams, R. T.; Qiu, Y. et al., Synthesis of Lead-Free $Cs_3Sb_2Br_9$ Perovskite Alternative Nanocrystals with Enhanced Photocatalytic CO_2 Reduction Activity. *Nanoscale* **2020,** *12*, 2987-2991.

(14) Liu, Y. W.; Guo, S. H.; You, S. Q.; Sun, C. Y.; Wang, X. L.; Zhao, L.; Su, Z. M., Mn-Doped $CsPb(Br/Cl)_3$ Mixed-Halide Perovskites for CO_2 Photoreduction. *Nanotechnology* **2020,** *31*, 215605.

(15) Dong, G.-X.; Zhang, W.; Mu, Y.-F.; Su, K.; Zhang, M.; Lu, T.-B., A Halide Perovskite as a Catalyst to Simultaneously Achieve Efficient Photocatalytic CO_2 Reduction and Methanol Oxidation. *Chem. Commun.* **2020,** *56*, 4664-4667.

(16) Wan, S. P.; Ou, M.; Zhong, Q.; Wang, X. M., Perovskite-Type $CsPbBr_3$ Quantum Dots/UiO-66(NH_2) Nanojunction as Efficient Visible-Light-Driven Photocatalyst for CO_2 Reduction. *Chem. Eng. J.* **2019,** *358*, 1287-1295.

(17) Shyamal, S.; Dutta, S. K.; Pradhan, N., Doping Iron in $CsPbBr_3$ Perovskite Nanocrystals for Efficient and Product Selective CO_2 Reduction. *J. Phys. Chem. Lett.* **2019,** *10*, 7965-7969.

(18) Pan, A.; Ma, X.; Huang, S.; Wu, Y.; Jia, M.; Shi, Y.; Liu, Y.; Wangyang, P.; He, L.; Liu, Y., $CsPbBr_3$ Perovskite Nanocrystal Grown on MXene Nanosheets for Enhanced Photoelectric Detection and Photocatalytic CO_2 Reduction. *J. Phys. Chem. Lett.* **2019,** *10*, 6590-6597.

(19) Mu, Y.-F.; Zhang, W.; Guo, X.-X.; Dong, G.-X.; Zhang, M.; Lu, T.-B., Water-Tolerant Lead Halide Perovskite Nanocrystals as Efficient Photocatalysts for Visible-

Light-Driven CO_2 Reduction in Pure Water. *ChemSusChem* **2019,** *12*, 4769-4774.

(20) Guo, X.-X.; Tang, S.-F.; Mu, Y.-F.; Wu, L.-Y.; Dong, G.-X.; Zhang, M., Engineering a $CsPbBr_3$-Based Nanocomposite for Efficient Photocatalytic CO_2 Reduction: Improved Charge Separation Concomitant with Increased Activity Sites. *RSC Advances* **2019,** *9*, 34342-34348.

(21) Guo, S.-H.; Zhou, J.; Zhao, X.; Sun, C.-Y.; You, S.-Q.; Wang, X.-L.; Su, Z.-M., Enhanced CO_2 Photoreduction *via* Tuning Halides in Perovskites. *J. Catal.* **2019,** *369*, 201-208.

(22) Sheng, J.; He, Y.; Li, J.; Yuan, C.; Huang, H.; Wang, S.; Sun, Y.; Wang, Z.; Dong, F., Identification of Halogen-Associated Active Sites on Bismuth-Based Perovskite Quantum Dots for Efficient and Selective CO_2-to-CO Photoreduction. *ACS Nano* **2020,** *14* (10), 13103-13114.